# Long-term variations of the nighttime electron density enhancement during the ionospheric midlatitude summer

AUTHOR(S):

Chen, C. H.; Saito, A.; Lin, C. H.; Liu, J. Y.

CITATION:

Chen, C. H. ...[et al]. Long-term variations of the nighttime electron density enhancement during the ionospheric midlatitude summer. Journal of Geophysical Research 2012, 117: A07313.

ISSUE DATE:

2012-07-19

URL:

http://hdl.handle.net/2433/160129

# Long-term variations of the nighttime electron density enhancement during the ionospheric mid-latitude summer

C. H. Chen[1], A. Saito[1], C. H. Lin[2], J. Y. Liu[3,4,5]

[1]Department of Geophysics, Graduate School of Science, Kyoto University, Kyoto, Japan
[2]Department of Earth Science, National Cheng Kung University, Tainan, Taiwan
[3]Institute of Space Science, National Central University, Chung-Li, Taiwan
[4]Center for Space and Remote Sensing Research, National Central University, Chung-Li, Taiwan
[5]National Space Organization, Taiwan

**Abstract**

This study, for the first time, presented the long-term variations of Mid-latitude Summer Nighttime Anomaly (MSNA) in the two hemispheres by using 66 ground-based ionosonde observations from 1957 to 2010. MSNA is characterized by the feature of higher nighttime electron density than daytime density in the mid-latitude region during local summer months. Observations from 66 ionosonde stations were used to calculate the MSNA index which is defined by the difference between nighttime and noontime *NmF2* values. The MSNA occurrence is determined by positive value of the MSNA index. The global distribution map of the MSNA index shows that there are three regions of intense MSNA. Three ionosonde stations in each of active MSNA regions were chosen to study the long-term variation of MSNA covering longer than one solar cycle. One station in the southern hemisphere is AIJ6N (Argentine IS; 65.2°S, 64.3°W geographic) and two stations in the northern hemisphere are LN047 (Lannion; 48.8°N, -3.4°E geographic) and MG560 (Magadan; 60.0°N, 151.0°E geographic). Results show that there is a clear solar activity negative dependence of the MSNA index, high MSNA in the low solar activity condition and low MSNA in the high solar activity condition. The seasonal and solar activity variations of the MSNA index are explained by the combined effects of the vertical plasma drift induced by the neutral wind and photoionization during the nighttime.

## 1. Introduction

The Weddell Sea Anomaly (WSA) of the Earth's ionosphere is characterized by the greater electron density in the nighttime than that in the daytime near the Weddell Sea region during the summer period. This nighttime electron density enhancement feature was firstly discovered by an ionosonde located nearby the region in 1950s [Bellchambers and Piggott, 1958; Penndorf, 1965; Dudeney and Piggott, 1978]. Recently, this feature was further observed by TOPEX/Poseidon [Horvath and Essex, 2003; Horvath, 2006; Jee et al., 2009], FORMOSAT-3/COSMIC [Burns et al., 2008; He et al., 2009; Lin et al., 2009, 2010], and CHAMP [Liu et al., 2010] satellites, indicating that the WSA extends over a much larger region between the South America and Antarctica. The global distribution maps of *NmF2* and *hmF2* calculated by FORMOSAT-3/COSMIC radio occultation were utilized to investigate the WSA [Burns et al., 2008]. Their results showed the enhanced electron densities accompanied by the increased height of the *F2* peak around WSA region during southern hemisphere summer. They suggested that the electron density enhancement of the WSA is associated with the *F2* peak altitude increasing. Using the observations of FORMOSAT-3/COSMIC measurements, Lin et al. [2009] constructed monthly global three-dimensional maps of the ionospheric electron density structures of the

48 WSA and reported that the WSA spans in a large region and is most significantly seen
49 at around 300 km altitude.

50 Regarding the occurrence of WSA during different solar activities, the total
51 electron content (TEC) observation by the TOPEX/Poseidon altimeter was used to
52 observe the spatial extent of the WSA over the ocean near the Antarctic Peninsula
53 during the high solar activity period in 1998 and 1999 [Horvath and Essex, 2003] and
54 the low solar activity period in 1996 and 1997 [Horvath, 2006]. Results showed that
55 the WSA occurred on both solar activity conditions. Jee et al. [2009] analyzed more
56 than 13-year global TOPEX TEC maps to further study the seasonal and solar cycle
57 variations of the WSA in the southern hemisphere. They presented that the WSA
58 appears only in the summer when F10.7 is low, but it appears in all seasons (except
59 for winter) when F10.7 is high. However, Liu et al. [2010] analyzed 6-year *in situ*
60 electron density measurements at 400 km from the CHAMP satellite and found that
61 the feature of WSA is more pronounced at solar minimum than at the solar maximum.
62 They suggested that the difference between their results and those in Jee et al. [2009]
63 may be due to different behavior between TEC and electron density at 400 km.

64 Not only in the southern hemisphere, recently, the nighttime electron density
65 enhancement was also observed in the northern hemisphere. Lin et al. [2009]
66 presented a WSA-like anomalous nighttime electron density enhancement in the

northern summer in June 2007 by the FORMOSAT-3/COSMIC data and the global ionospheric map (GIM-TEC). Thampi et al. [2009] used tomographic observations over Japan to investigate the northern electron density anomaly around the East Asian region during July-August 2008. They found that the anomaly in the northern hemisphere are absent at lower altitudes ( < 275 km) and appear at higher altitudes ( ~ 275 - 550 km). Both WSA in the southern hemisphere and the similar anomalies in the northern hemisphere appear around magnetic mid-latitude regions and local summer nighttime, these anomalies are, therefore, named as the Mid-latitude Summer Nighttime Anomaly (MSNA) [Thampi et al., 2009]. Later, Liu et al. [2010] reported that global distribution of nighttime electron enhancements at East Asian (around geographic 53°N and 150°E), Northern Atlantic (around geographic 45°N and -50°E), and South Pacific (around geographic -60°N and -110°E) regions by using CHAMP satellite data. Lin et al. [2010] presented similar electron density anomalous feature in the Northeast Asia and Europe/Africa longitudes of the northern hemisphere by using the electron density at 300 km altitude from FORMOSAT-3/COSMIC observations. Liu et al. [2010] and Lin et al. [2010] also suggested that this nighttime electron density enhancement is a general mid-latitude feature that exists at longitudes where the magnetic equator is apart from the geographic equator.

Regarding to the solar cycle variation of MSNA in the northern hemisphere, Liu et al. [2010] used 6 years of *Ne* data at 400 km by CHAMP satellite and found that the MSNA is more pronounced at solar minimum than at solar maximum. However, they used only 6-year data, which is hardly to discuss the solar activity dependent. Also, a quantitatively analytical method is needed for the long-term variations of MSNA in place of observation by naked eye. In this paper, we defined a MSNA strength index (MSNA index) from ratio difference between the nighttime and noontime electron densities to investigate the long-term variations of the MSNA quantitatively in the two hemispheres. According to previous studies [Horvath 2006; He et al., 2009; Thampi et al., 2009; Lin et al., 2010; Liu et al., 2010; Chen et al., 2011], the neutral wind effect may play a critical role in the nighttime electron density enhancement. The neutral wind effect along the magnetic field line and the associated seasonal and solar activity dependence of the MSNA were investigated by using the model estimations based on the Horizontal Wind Model 93 (HWM93; Hedin et al., 1996), the International Geomagnetic Reference Field (IGRF-10; Maus et al., 2005), and SAMI2 (Sami2 is Another Model of the Ionosphere; Huba et al., 2000) model.

## 2. Data

In order to study the occurrence and the amplitude of MSNA, a MSNA index is defined in this study. The MSNA index is defined as ratio difference between the

104 nighttime daily maximum value of *NmF2* and the noontime (12:00 LT) one divided by
105 the daily minimum *NmF2*. The MSNA index denotes the percentage of nighttime
106 electron density enhancement compared with the daytime electron density.

107 $$\text{MSNA index (\%)} = \frac{Max(NmF2)_{night} - NmF2_{12LT}}{Min(NmF2)_{all}} \times 100 \quad (1)$$

108 The nighttime is defined by 19:00 LT - 04:00 LT during the local summer and is
109 defined by the time when the solar zenith angle at 300 km is greater than 90° during
110 other seasons. We further exclude the data when the decrease curve of NmF2 value
111 occurs during the nighttime. The positive MSNA index indicates occurrence of the
112 nighttime electron density anomaly/enhancement and the greater MSNA index
113 amplitude indicates a stronger MSNA feature. The MSNA index can be a proxy for
114 the long-term study of the MSNA quantitatively. The *NmF2* data of 66 ionosonde
115 stations around mid-latitude region were used to calculate the distribution map of the
116 MSNA index during 1957 - 2010. Figure 1 shows the locations of 66 ionosonde
117 stations and their median value of MSNA index during local summer months
118 (May-Jul. for northern hemisphere; Nov.-Jan. for southern hemisphere). It can be seen
119 that the positive MSNA indexes appear between South America and Antarctica region
120 (a typical Weddell Sea Anomaly feature), West European and East America region
121 (Atlantic Ocean), and Northeast Asian regions. The occurrence regions of the MSNA
122 are consistent with previous studies [Liu et al., 2010; Lin et al., 2010]. In Figure 1, the

123 maximum value of MSNA index is about 53% in the southern hemisphere, which is
124 larger than that in the northern hemisphere (about 36% around Northeast Asian
125 region). The values of MSNA index around Northeast Asian region are larger than that
126 around West European region. We choose three most representative ionosonde
127 stations at each MSNA region to study the long-term variations of the MSNA feature.
128 Data from three ionosonde located around geomagnetic mid-latitude region with
129 station codes listed as AIJ6N (in the southern hemisphere), LN047 and MG560 (both
130 are in the northern hemisphere) are analyzed. Table 1 shows the IGRF-10 geographic
131 and geomagnetic coordinates of the three ionosondes.

132 Figure 2 shows daily variations of the solar activity F10.7 index (top panel) and
133 the ionospheric *NmF2* values measured by AIJ6N (Figure 2a), LN047 (Figure 2b),
134 and MG560 (Figure 2c) ionosonde stations. The data period, 1974-1988, was chosen
135 because all these three stations had continuous data during that period. The solar
136 activity dependence of the overall *NmF2* is clearly seen in Figures 2a-2c. Figure 2a
137 shows the feature of higher nighttime *NmF2* value than daytime *NmF2* value around
138 December solstice (the local summer) in the southern hemisphere. The similar feature
139 is also found in Figures 2b and 2c around June solstice in the northern hemisphere but
140 less discernible than that of the southern hemisphere.

141 Subdividing data into various seasons during the period (listed in Table 1), the
142 seasonal variations of *NmF2* at the three stations in M-month (Feb.-Apr.; in blue lines),
143 J-month (May-Jul.; in black-dot lines), S-month (Aug.-Oct.; in red dash lines), and
144 D-month (Nov.-Jan.; in pink-dot lines) are shown in Figure 3. Results show that the
145 MSNA appears in the southern hemisphere during D-month and lasts for couple hours
146 after 24:00 LT (Figure 3a). In Figures 3b and 3c, the stations in the northern
147 hemisphere, the MSNAs appear during the J-month and reach their maximum electron
148 density around 20:00 LT and 22:00 LT, respectively. The local time dependence of
149 MSNA in the southern hemisphere (Figure 3a) is different from those in the northern
150 hemisphere (Figures 3b and 3c). The more detailed daily variation of *NmF2* during
151 the local summer months and its average value at low solar activity and high solar
152 activity at these three stations are shown in Appendix A.

153 The daily variations of MSNA index at the three stations from 1971 to 1989 are
154 shown in Figure 4. It can be found that the MSNA indices are positive during the local
155 summer months in the both hemispheres. Comparing with the F10.7 index (top panel
156 in Figure 2), the values of MSNA index at AIJ6N (Figure 4a) show a negative
157 correlation to the solar activity, high/low MSNA index during low/high solar activity
158 period. This feature is also seen in LN047 (Figure 4b) and MG560 (Figure 4c)
159 stations.

160 The monthly median MSNA index values and MSNA occurrence rates are shown
161 in Figure 5 during the high (F10.7 $\geqq$ 120; in black bar) and the low (F10.7 < 120; in
162 gray bar) solar activity periods. It is noted that we excluded days when the sum of Kp
163 index is larger than 240 per day to avoid the magnetic storm effects. The seasonal and
164 solar activity variations of MSNA index amplitudes are shown in Figures 5a-5c. They
165 show that the MSNAs appear during November to February at AIJ6N station (Figure
166 5a), during May to July at LN047 station (Figure 5b), and during May to August at
167 MG560 station (Figure 5c). The results in Figures 5a-5c indicate that the MSNA index
168 amplitudes and the MSNA periods in the low solar activity are larger and longer than
169 that in the high solar activity. It also shows that the maximum MSNA indexes in the
170 northern hemisphere are weaker/smaller than that in the southern hemisphere. The
171 monthly MSNA occurrence day (the day of positive MSNA index) was counted
172 during the high and low solar activity periods to study the seasonal and solar activity
173 dependences of the MSNA occurrence rate (Figures 5d-5f). We can see that there are
174 high MSNA occurrence rate during the local summer months at the three stations. It
175 also shows the negative solar activity dependence of MSNA occurrence rate, high
176 occurrence rate during the low solar activity period. The maximum occurrence rate
177 during low solar activity period can reach around 40%, 35%, and 40% at AIJ6N,
178 LN047, and MG560 stations, respectively. However, during high solar activity period,

179 the maximum occurrence rates are reduced by around 5% - 10%.

180 **3. Discussion**

181 Although the WSA in the southern hemisphere was discovered in 1950s and the
182 associated physical mechanisms were discussed in later literatures [c.f. Burns et al.,
183 2008 and references therein], recent renewed observations give wider extended
184 coverage of the anomaly and prompt us to investigate the physical mechanism based
185 on these new observations. According to the previous studies, the possible physical
186 mechanisms of MSNA are photoionization of solar ultraviolet radiation [Sojka et al.,
187 1985; Horvath and Essex, 2003], equatorward neutral winds [Park, 1971; Dudeney
188 and Piggott, 1978; Su et al., 1994; Horvath and Essex, 2003; He et al., 2009; Thampi
189 et al., 2009; Liu et al., 2010; Lin et al., 2010; Chen et al., 2011], the magnetic field
190 configuration and offset effect [Khol and King, 1967; Dudeney and Piggott, 1978;
191 Horvath, 2006; Lin et al., 2009; 2010; Liu et al., 2010; Chen et al., 2011], and the
192 downward diffusion of the plasmaspheric plasma [Park, 1971; Bailey et al., 1991;
193 Burns et al., 2008; Liu et al., 2010; Chen et al., 2011]. Recently, Chen et al. [2011]
194 used a theoretical model, SAMI2 model [Huba et al., 2000], to reproduce the
195 integrated three-dimensional WSA electron density structure and examine the causal
196 mechanisms of WSA formation. Comparing with different neutral wind conditions,
197 their results found that the equatorward neutral wind in the nighttime is the most

198 important driver for the WSA formation. The equatorward neutral wind can sustain
199 the ionospheric layer at higher altitude to maintain a longer lifetime for the electron
200 density. On the other hand, the most important plasma source in the ionosphere is the
201 photoionization rate. Around the latitude of the WSA region, the longer time of
202 photoionization due to later sunset can provide the plasma source in the nighttime
203 ionosphere. As a result, the combined effects of the geomagnetically equatorward
204 neutral wind and the longer time of photoionization rate result in the intensity of the
205 WSA density structure in the mid-latitude nighttime. According to the parameters by
206 Chen et al. [2011], Figure 6 shows the global distribution of MSNA index by SAMI2
207 model in 2007 on Jun. 16 in the northern hemisphere and Dec. 16 in the southern
208 hemisphere. Similar with the ionosonde *NmF2* observation data, three MSNA regions
209 are seen around South American, West European, and Northeast Asian. However,
210 SAMI2 model results show high MSNA index around West European then Northeast
211 Asian and also the feature of MSNA is not clear around Northeast Asian region, which
212 are different with the observation results.

213 **3.1 Neutral wind and photoionization rate effects**

214 The dominant feature of the mid-latitude neutral wind at 300 km altitude is
215 equatorward flow in the nighttime and poleward flow in the daytime [Kawamura et al.,
216 2000; Liu et al., 2003; Kil et al., 2006]. The nighttime equatorward neutral wind flow

can transport ionospheric plasma to higher altitudes along the geomagnetic field lines, which will preserve plasma for a long time by the lower recombination rate. The poleward neutral wind flow will transport ionospheric plasma to lower altitudes and increase the plasma loss by the high recombination rate. In order to discuss the neutral wind effect for the variations of MSNA, the configuration of the neutral wind and the geomagnetic field line, such as declination and inclination angles, should be considered. The vertical component of the neutral wind along the magnetic field line at 300 km altitude can be calculated by

$$V_{vert} = \mp(W_m^{geo}\cos\theta + W_z^{geo}\sin\theta)\cos|I|\sin|I| \quad (2)$$

Where

$V_{vert}$ = vertical component of the plasma drift (positive for upward);

$\mp$ = magnetic northern/southern hemisphere;

$W_m^{geo}$ = the geographically meridional neutral wind velocity (positive for northward);

$W_z^{geo}$ = the geographically zonal neutral wind velocity (positive for eastward);

$\theta$ = declination angle of the geomagnetic field (positive for eastward);

$I$ = inclination angle of the geomagnetic field (positive for northern hemisphere; negative for southern hemisphere).

The photoionization rate at 300 km altitude was calculated by the SAMI2 model. The positive value of photoionization rate can provide new plasma in the ionosphere.

236 Figure 7 shows the local time variations of vertical component of plasma drift induced
237 by the neutral wind (HWM-93; Hedin et al., 1996) along the magnetic field line
238 (black-dot line) as well as the photoionization rate (blue-dot line) at AIJ6N (Figures
239 7a and 7d), LN047 (Figures 7b and 7e), and MG560 (Figures 7c and 7f) in June
240 (Figures 7a-7c) and December (Figures 7d-7f) in 1985. It can be seen that in Figures
241 7a and 7d, the vertical plasma drifts are upward after 16:00 LT in June and December
242 and reach their maximum values around 20:00 LT before the midnight. During
243 December month of AIJ6N station, the photoionization rate remains positive during
244 the entire day. However, the photoionization rates in June month are positive value
245 only during the daytime, 08:00 - 16:00 LT. The stations in the northern hemisphere
246 show a long time of photoionization and upward plasma drift during the nighttime in
247 June month. Combining these two effects, we suggest that MSNAs prefer to occur at
248 the condition with the upward plasma drift and the positive photoionization rate
249 during the nighttime period. We defined the effective period with positive vertical
250 plasma drift and positive photoionization rate during the nighttime period to study
251 these effects for the long-term variation of MSNA. This effective period are called as
252 the ionization-uplift effect in this study and shown by gray color in Figure 7.

253 $$\text{ionization-uplift effect} = \sum_{t=19}^{04} V_{vert} \cdot \Delta t \cdot \delta_t / 1000 \qquad (3)$$

254 Where, $\delta_t$ is equal 0 at all the time but is equal 1 when the photoionization rate

larger than 0 at the time, t. The dimension of ionization-uplift effect is distance (km). The larger ionization-uplift effect indicates the variation of plasma density affected by both stronger plasma drift and photoionization rate.

### 3.2 Seasonal variation

The ionosonde results in the southern hemisphere in Figures 3a, 5a, and 5d reveal that the nighttime electron density enhancements prefer to appear during summer months than winter months, which are consistent with the previous studies [Bellchambers and Piggott, 1958; Penndorf, 1965; Dudeney and Piggott, 1978; Burns et al., 2008; Lin et al., 2009; Liu et al., 2010]. Liu et al. [2010] and Chen et al. [2011] reported that the neutral wind is an important driver for the MSNA formation. In December month, the large upward plasma drift induced by the neutral wind and positive photoionization rate (large ionization-uplift effect) during the nighttime (Figure 7d) resulted in the formation of MSNA (Figures 3a and 5a). In June month, although there is a large upward plasma drift appearing during the nighttime (Figure 7a) but there is no photoionization. As a result, no MSNA appeared during this month (Figures 3a and 5a). It seems that the longer time of the photoionization rate, which can prove electron density source around 300 km altitude in the nighttime, is another important factor for the MSNA formation.

Not only in the southern hemisphere, but also in the northern hemisphere the

features of nighttime electron density enhancement were seen around West European and Northeast Asian regions. Lin et al. [2009] used FORMOSAT-3/COSMIC data to construct the electron density slices at various altitudes and longitudes at 22:00 LT in June 2007. They also compared with global ionospheric maps (GIM) data and found that the feature of the anomalous election density enhancement appear around Northeast part of the Asian region. It is worth to note that in the Figure 4 of Lin et al. [2009], there is a clearly but weak MSNA phenomenon around West European area, although it was not mentioned by the authors. Liu et al. [2010] calculated the density differences between the daytime (12:00 LT) and the nighttime (22:00 LT) at 400 km altitude by CHAMP satellite data in the December and June solstices. They found that there are two anomalous regions appearing in the northern hemisphere in East Asia (EA) sector and North Atlantic (NA). In this study, we calculated the distribution of the MSNA index and found two high value regions of the MSNA index in the northern hemisphere around West European and Northeast Asian regions as shown in Figure 1. The seasonal variation of *NmF2* in Figure 3, the seasonal variation of the MSNA index in Figures 5a-5c, and the occurrence rate of MSNA in Figures 5d-5f are consistent with the MSNA distributions revealed in the previous studies. The value of ionization-uplift effect at LN047 (Figures 7b and 7e) and MG560 (Figures 7c and 7f) are high in June month (Figures 7b and 7c) and zero in December month (Figures 7e

293 and 7f), similar seasonal variation with AIJ6N station. The monthly variation of the
294 MSNA index (Figures 5b and 5c) and the MSNA occurrence (Figure 5e and 5f) also
295 show seasonal variation, high values during summer months and low values during
296 winter months. This implies that the evolution of combined effect by the vertical
297 plasma drift induced by the neutral wind and the solar photoionization rate can
298 potentially explain the seasonal variation of MSNA.

299 **3.3 Solar activity variation**

300 The solar cycle variation of WSA in the southern hemisphere had been studied
301 by Jee et al. [2009] with TOPEX TEC observation data. Their results showed that
302 WSA occurs more frequently during high solar activity period than low solar activity
303 period. However, using electron density data at 400 km by CHAMP satellite, Liu et al.
304 [2010] found that WSA in the southern hemisphere occurred around August-March
305 during high and low solar activity conditions, nearly independent of solar activity.
306 Their results further showed that the occurrence period of MSNA in the northern
307 hemisphere was longer in the low solar activity condition than in the high solar
308 activity condition. In this study, the occurrence rate of MSNA at the two hemisphere
309 stations (Figures 5d-5f) show a clear solar activity dependence, high occurrence rate
310 during the low solar activity period and low occurrence rate during the high solar
311 activity period. Also, the strength of MSNA shows the solar activity dependence

312 (Figures 5a-5c), high value during the low solar activity period than that during the
313 high solar activity period, except for MG560 station (Figure 5c).

314 In order to discuss the solar activity dependence of MSNA, the MSNA index at
315 each ionosonde station during several years (listed in Table 1) were used to examine
316 their relationship to the solar activity F10.7 index. Figure 8 presents the linear
317 regressions of the F10.7 index versus the MSNA index and the ionization-uplift effect
318 in the two hemispheres. Figures 8a, 8d, and 8g show the relationships between the
319 F10.7 index and the MSNA index. Results show that the correlation coefficients are
320 negatively high values at AIJ6N and LN047 stations but negatively moderate value at
321 MG560 station. This solar activity dependence also can be seen in Figure 5 and
322 generally has a good agreement with previous study [Liu et al., 2010].

323 Figures 8b, 8e, and 8h present the relationships between the F10.7 index and the
324 ionization-uplift effect. It is shown that the negatively high correlation coefficients at
325 AIJ6N and LN047 stations and negatively moderate correlation coefficient at MG560
326 station. Similar with the MSNA index, the ionization-uplift effect has the negative
327 solar activity dependence. This is due to that the neutral wind velocity in the
328 mid-latitude nighttime is high during the low solar activity period and low during the
329 high solar activity period [Kawamura et al., 2000]. Faster neutral wind could induce

330 faster vertical plasma drift and then result in higher electron density in the
331 mid-latitude ionosphere.

332 Figures 8c, 8f, and 8i show relationship between the MSNA index and the
333 ionization-uplift effect. It shows that the MSNA index is proportional to the
334 ionization-uplift effect, except for MG560 station. The high correlation coefficients
335 show that a larger ionization-uplift effect results in a larger MSNA index, suggesting
336 that the combined effect by the plasma drift and the photoionization rate play an
337 important role for the generation of MSNA in different solar activity conditions. On
338 the other hand, the correlation coefficient is high at LN047 station but low at MG560
339 station. This different feature between LN047 and MG560 implies that the mechanism
340 of ionization-uplift effect cannot fully explain the solar activity variation of MSNA in
341 the northern hemisphere. It is possibly due to the accuracy of the neutral wind model
342 or the effect of the plasma downward diffusion from the plasmasphere during the
343 nighttime in the mid-latitude ionosphere. The recombination rate in the nighttime may
344 also affect the variation of MSNA in the ionosphere. However, it needs a further study
345 by using a theoretical model together with the plasmaspheric data by satellite
346 observations.

347 The feature of MSNA seen in Figures 1, 4, and 5 show a hemispheric difference,
348 large MSNA index in southern hemisphere summer than that in northern hemisphere

summer. Results presented by Lin et al. [2009; 2010], He et al. [2009], and Liu et al. [2010] also showed this hemispheric asymmetry. The occurrence rates of MSNA (Figures 5d-5f) in the southern hemisphere are larger than that in the northern hemisphere. The amplitudes of the MSNA index (Figure 5a-5c) also show the high value in the southern hemisphere, except for MG560 at the high solar activity condition. The similar feature can be seen in Figure 7. It is shown that the value of ionization-uplift effect during the southern hemisphere December month is larger than that during the northern hemisphere June month. This implies that there is more upward plasma induced by the neutral wind and more photoionization in the WSA region than the regions in the northern hemisphere resulting in the more distinct anomaly seen in the WSA region. The hemispheric difference of the MSNA index seems can be directly explained by the strength of the combined effect by the plasma drift and the photoionization rate.

Regarding to the longitudinal variations of MSNA in the northern hemisphere, the MSNA index shown in Figures 1, 4, and 5 reveal that the MSNA index around Northeast Asia region (MG560) is larger than that around West European region (LN047) during May and August in high and low solar activity conditions. The occurrence rate of MSNA at MG560 (Figure 5f) is also larger than that at LN047 (Figure 5e) during May and August. These results reveal the longitudinal variation of

368 MSNA in the northern hemisphere. Since the meridional neutral wind is the most
369 important factor to control the occurrence of MSNA [Chen et al., 2011], the
370 longitudinal variation of MSNA may be caused by the declination and inclination of
371 the magnetic field [He et al., 2009; Liu et al., 2010]. On the other hand, the
372 longitudional feature (differences value in the MSNA index and the occurrence of
373 MSNA between West European and Northeast Asian) is more distinct during the high
374 solar activity period than during the low solar activity period (Figure 5). Burns et al.
375 [2008] suggested that the evening downward flux of plasma from the plasmasphere
376 may also affect the formation of WSA. According to the results in Figure 5, the solar
377 activity dependence of the MSNA longitudinal structure may result from the
378 plasmaspheric downward diffusion in the mid-latitude ionosphere. Figure 6 shows the
379 quickly results of MSNA global distribution by SAMI2 model. Comparing with the
380 ionosonde *NmF2* results (Figure 1), the model result shows similar longitudinal
381 structure of MSNA but the MSNA amplitude around the Northeast Asian region is
382 smaller than the West European region. Figure 9 further shows the correlated plasma
383 diffusion velocities at the West European (50°N, -5°E, black-dot line) and the
384 Northeast Asian (60°N, 150°E, gray-dot line) locations. It is clearly shown that there
385 is a large downward velocity at the West European location during the nighttime,
386 which can provide the plasma source in the nighttime to maintain the longer time of

387 plasma. The feature of downward plasma diffusion is not clearly at the Northeast
388 Asian location, which is the possible reason to cause the weak MSNA feature here.
389 However, it needs further theoretical studies using by plasmasphere-ionosphere
390 models.

391 **4. Summary**

392 This paper utilized the long-term ionosonde *NmF2* data to study the features of
393 ionospheric mid-latitude summer nighttime anomalies (MSNAs) in the two
394 hemispheres and their seasonal and solar activity dependences. MSNA index was
395 defined to study the long-term variations of MSNA quantitatively. Results show
396 clearly seasonal and solar cycle variations of MSNA in the two hemispheres. The
397 quasi-linear relationships between the MSNA index and the F10.7 index present the
398 clear solar activity dependence of MSNA, negatively high correlation at AIJ6N and
399 LN047 station but negatively moderate correlation at MG560 station. These long-term
400 variations of MSNA can be explained by the combined effect of the plasma drift
401 induced by the neutral wind and the photoionization rate. However, the different
402 correlation coefficients between West European region and Northeast Asian region
403 indicate that the formation of MSNA in the northern hemisphere cannot fully be
404 explained by the combined effect. The solar activity and season dependences of
405 downward diffusion of plasma from the plasmasphere during the nighttime may affect

406 the variation of MSNA and caused the longitudinal structure of MSNA in the northern
407 ionosphere. The nighttime recombination rate around F-region may also cause the
408 variation of MSNA in different solar activity conditions. Thus, it may be the possible
409 mechanisms responsible to the smaller correlation coefficient around the Northeast
410 Asian region. A comprehensive study taking into account of these possible effects by
411 the observation and/or model simulation is needed in the future work.

412 **Acknowledgments**

413 C. H. Chen is supported by Interchange Association, Japan (IAJ). The authors are
414 grateful to Dr. T. Maruyama and Dr. T. Tsugawa of National Institute of Information
415 and Communications Technology (NICT), Japan, for the helpful comments for this
416 paper. The F10.7 data are downloaded from the Space Physics Interactive Data
417 Resource (SPIDR) web: http://spidr.ngdc.noaa.gov/. The ionosonde data are provided
418 by SPIDR and NICT.

419

420 **Reference**

421 Bailey, G. J., R. Sellek, N. Balan (1991), The effects of interhemispheric coupling on
422 night-time enhancements in ionospheric total electron content during winter at
423 solar minimum, Ann. Geophys., 9, 738-747.
424 Bellchambers, W. H., and W. R. Piggott (1958), Ionospheric measurements made at
425 Halley Bay, Nature, 182, 1596-1597.
426 Burns, A. G., Z. Zeng, W. Wang, J. Lei, S. C. Solomon, A. D. Richmond, T. L. Killen,
427 and Y.-H. Kuo (2008), The behavior of the F2 peak ionosphere over the South
428 Pacific at dusk during quiet summer condition from COSMIC data, J. Geophys.
429 Res., 113, A12305, doi:10.1029/2008JA013308.
430 Chen, C. H., J. D. Huba, A. Saito, C. H. Lin, and J. Y. Liu (2011), Theoretical study
431 of the ionospheric Weddell Sea Anomaly using SAMI2, J. Geophys. Res., 116,
432 A04305, doi:10.1029/2010JA015573.
433 Dudeney, J. R., and W. R. Piggott (1978), Antarctic ionospheric research, in Upper
434 Atmosphere Research in Antarctica, Ant. Res. Ser., edited by L. J. Lanzerotti
435 and C. G. Park, pp. 200-235, AGU, Washington, D.C.

He, M., L. Liu, W. Wan, B. Ning, B. Zhao, J. Wen, X. Yue, and H. Le (2009), A study of the Weddell Sea Anomaly observed by FORMOSAT-3/COSMIC, J. Geophys. Res., 114, A12309, doi:10.1029/2009JA01417.

Hedin, A. E., E. L. Fleming, A. H. Manson, F. J. Schmidin, S. K. Avery, R. R. Clark, S. J. Franke, G. J. Fraser, T. Tsuda, F. Vial, and R. A. Vincent (1996), Empirical wind model for the upper, middle and lower atmosphere, J. Atmos. Terr. Phys., 58, 1421-1427.

Horvath, I. and E. A. Essex (2003), The Weddell sea anomaly observed with the Topex satellite data, J. Atmos. Sol. Terr. Phys., 65, 693-706.

Horvath, I. (2006), A total electron content space weather study of the nighttime Weddell Sea Anomaly of 1996/1997 southern summer with TOPEX/Poseidon radar altimetry, J. Geophys. Res., 111, A12317, doi:10.1029/2006JA011679.

Huba, J. D., G. Joyce, and J. A. Fedder (2000), Sami2 is Another Model of the Ionosphere (SAMI2): A new low-latitude ionosphere model, J. Geophys. Res., 105, 23035-23053.

Jee, G., A. G. Burns, Y.-H. Kim, and W. Wang (2009), Seasonal and solar activity variations of the Weddell Sea Anomaly observed in the TOPEX total electron content measurements, J. Geophys. Res., 114, A04307, doi:10.1029/2008JA013801.

Kawamura, S., Y. Otsuka, S.-R. Zhang, and S. Fukao (2000), A climatology of middle and upper atmosphere radar observations of thermospheric winds, J. Geophys. Res., 105, 12777-12788.

Kil, H., R. DeMajistre, L. J. Paxton, and Y. Zhang (2006), Nighttime F region morphology in the low and middle latitudes seen from DMSP F15 and TIMED/GUVI, J. Atmos. Sol. Terr. Phys., 68, 1672-1681, doi:10.1016/j.jastp.2006.05.024.

Kohl, H., J. W. King (1967), Atmospheric winds between 100 and 700 km and their effects on the ionosphere, J. Atmos. and Terr. Phys., 29, 1045-1062.

Lin, C. H., J. Y. Liu, C. Z. Cheng, C. H. Chen, C. H. Liu, W. Wang, A. G. Burns, and J. Lei (2009), Three-dimensional ionospheric electron density structure of the Weddell Sea Anomaly,J. Geophys. Res., 114, A02312, doi:10.1029/2008JA013455.

Lin, C. H., C. H. Liu, J. Y. Liu, C. H. Chen, A. G. Burns, and W. Wang (2010), Mid-Latitude Summer Nighttime Anomaly of the Ionospheric Electron Density Observed by FORMOSAT-3/COSMIC, J. Geophys. Res., 115, A033038, doi:10.1029/2009JA014084.

Liu, L., X. Luan, W. Wan, B. Ning, and J. Lei (2003), A new approach to the derivation of dynamic information from ionosonde measurements, Ann. Geophys., 21, 2185-2191.

Liu, H., S. V. Thampi, and M. Yamamoto (2010), Phase reversal of the diurnal cycle in the midlatitude ionosphere, J. Geophys. Res., 115, A01305, doi:10.1029/2009JA014689.

Maus, S., S. Macmillan, T. Chernova, S. Choi, D. Dater, V. Golovkov, V. Lesur, F. Lowes, H. Lühr, W. Mai, S. McLean, N. Olsen, M. Rother, T. Sabaka, A. Thomson, T. Zvereva (2005), The 10th generation international geomagnetic reference field, Physics of the Earth and Planetary Interiors, 151, 320-322.

Park, C. G. (1971), Westward electric fields as the cause of night-time enhancements in electron concentrations in mid-latitude F region, J. Geophys. Res., 76, 4560-4568.

Penndorf, R. (1965), The average ionospheric conditions over the Antarctic, in Geomagnetism and Aeronomy, Ant. Res. Ser., vol. 4, edited by A. H. Waynick, pp. 1-45, AGU, Washington, D.C.

Sojka, J. J., W. J. Raitt, R. W. Schunk, and J. L. Parish (1985), Diurnal variations of the dayside, ionospheric, mid-latitude trough in the southern hemisphere at 800 km: Model and measurement comparison, Planet. Space Sci., 33, 1375-1382.

Su, Y. Z., G. J. Bailey, N. Balan (1994), Night-time enhancements in TEC at equatorial anomaly latitudes, J. Atmos. and Terr. Phys. 56, 1619-1628.

Thampi, S., C. H. Lin, H. Liu, and M. Yamamoto (2009), First tomospheric observations of the mid-latitudes summer night anomaly (MSNA) over Japan, J. Geophys. Res., 114, A10318, doi:10.1029/2009JA014439.

## Caption

**Figure 1.** Location of 66 ionosondes and their median value of MSNA index during local summer months.

**Figure 2.** The daily variations of the 10.7 cm solar radio flux, F10.7 index (in unit of $10^{-22}Wm^{-2}Hz^{-1}$), and the NmF2 at (a)AIJ6N, (b)LN047, and (c)MG560 stations during 1971 to 1989.

**Figure 3.** Monthly variation of diurnal NmF2 at (a) AIJ6N, (b) LN047, and (c) MG560 stations in M-month (blue line), J-month (black-dot line), S-month (red dash line), and D-month (pink-dot line).

**Figure 4.** Daily variations of the positive MSNA index at (a) AIJ6N, (b) LN047, and (c) MG560 stations during 1971 to 1989.

**Figure 5.** Monthly variation of MSNA index values and MSNA occurrence rates. The monthly variation of MSNA indexes are shown at (a) AIJ6N, (b) LN047, and (c) MG560 stations in different solar activity conditions. Black bars indicate the high solar activity (F10.7 $\geqq$ 120) data and gray bars indicate the low solar activity (F10.7 $<$ 120) data. The monthly occurrence rates of MSNA are shown at (d) AIJ6N, (e) LN047, and (f) MG560 stations in different solar activity conditions. Black bars indicate the high solar activity (F10.7 $\geqq$ 120) data and gray bars indicate the low solar activity (F10.7 $<$ 120) data.

**Figure 6.** Global MSNA index during local summer days (Jun.16 for the northern hemisphere and Dec. 16 for the southern hemisphere) simulated by SAMI2 model. The black line indicates the geomagnetic equator.

**Figure 7.** Hourly variation of vertical neutral wind and photoionization rate. Top panels show the results at (a) AIJ6N, (b) LN047, and (c) MG560 stations in June month. Bottom panels show the results at (d) AIJ6N, (e) LN047, and (f) MG560 stations in December month. Black-dot lines and associated left-side y-axis indicate the vertical neutral wind. Blue-dot lines and associated right-side y-axis indicate the photoionization rate. Gray region indicate the ionization-uplift effect with upward neutral wind and positive photoionization rate.

**Figure 8.** Solar activity variations of the MSNA index and the ionization-uplift effect. The top three panels indicate the results at AIJ6N station (a-c). The middle three panels indicate the results at LN047 station (d-f). The bottom three panels indicate the results at MG560 station (g-i). The solar activity dependences of the MSNA index and the ionization-uplift effect are shown in the left three panels and the middle three panels, respectively. The relationship between the MSNA index and the ionization-uplift effect are shown in the right three panels. Red dash-lines indicate the linear regression lines and CC indicates the correlation coefficient.

**Figure 9.** Plasma velocities at 500 km altitude at West European and Northeast Asian locations on Jun. 16 in 2007 by SAMI2 model. The black-dot and gray-dot lines indicate the data at (50°N, -5°E) and (60°N, 150°E), respectively. Positive/negative value means the up/downward velocity.

548 **Figure A1.** The daily variation of *NmF2* (in gray lines) during the local summer
549 months and its average value (black-dot lines) at low solar activity (F10.7 index
550 smaller than 120, top three panels) and high solar activity (F10.7 index larger than
551 120, bottom three panels) at AIJ6N, LN047, and MG560 stations.

552 Table1. The locations of ionosonde stations used in this paper and those magnetic file
553 line parameters at 300 km altitude by IGRF-10 model in 1980.

| Code | Name | GLat | GLong | MLat. | inc. | dec.* | Data period |
|---|---|---|---|---|---|---|---|
| AIJ6N | Argentine IS | -65.2°N | -64.3°E | 48.99°S | -58.90° | 16.06° | 1958-1959,1962-1995 |
| LN047 | Lannion | 48.8°N | -3.4°E | 45.30°N | 63.98° | -7.28° | 1971-1989 |
| MG560 | Magadan | 60.0°N | 151.0°E | 52.96°N | 70.94° | -8.37° | 1968-2006,2009 |

554 * Positive value for east ward and negative value for west ward.

555 **Appendix A**

556 In this appendix, we analyze the daily variation of *NmF2* during the local summer
557 months as well as its average value and the solar activity variation of *NmF2* at AIJ6N,
558 LN047, and MG560 stations. It is clearly show that the averages *NmF2* have similar
559 variation during high and low solar activity conditions and the MSNA features occur
560 during the both solar activity conditions.

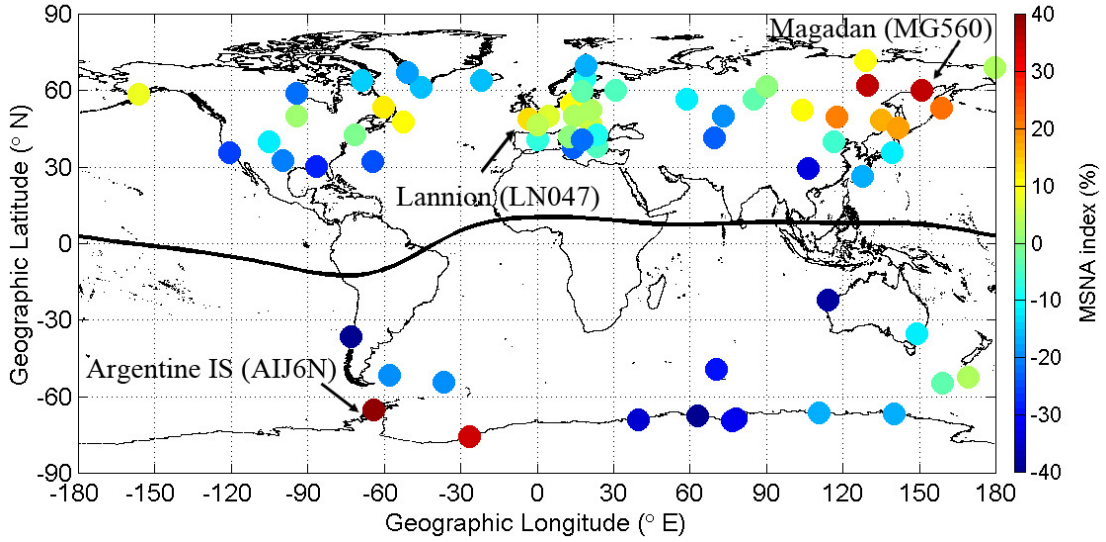


**Figure 1.** Location of 66 ionosondes and their median value of MSNA index during local summer months.

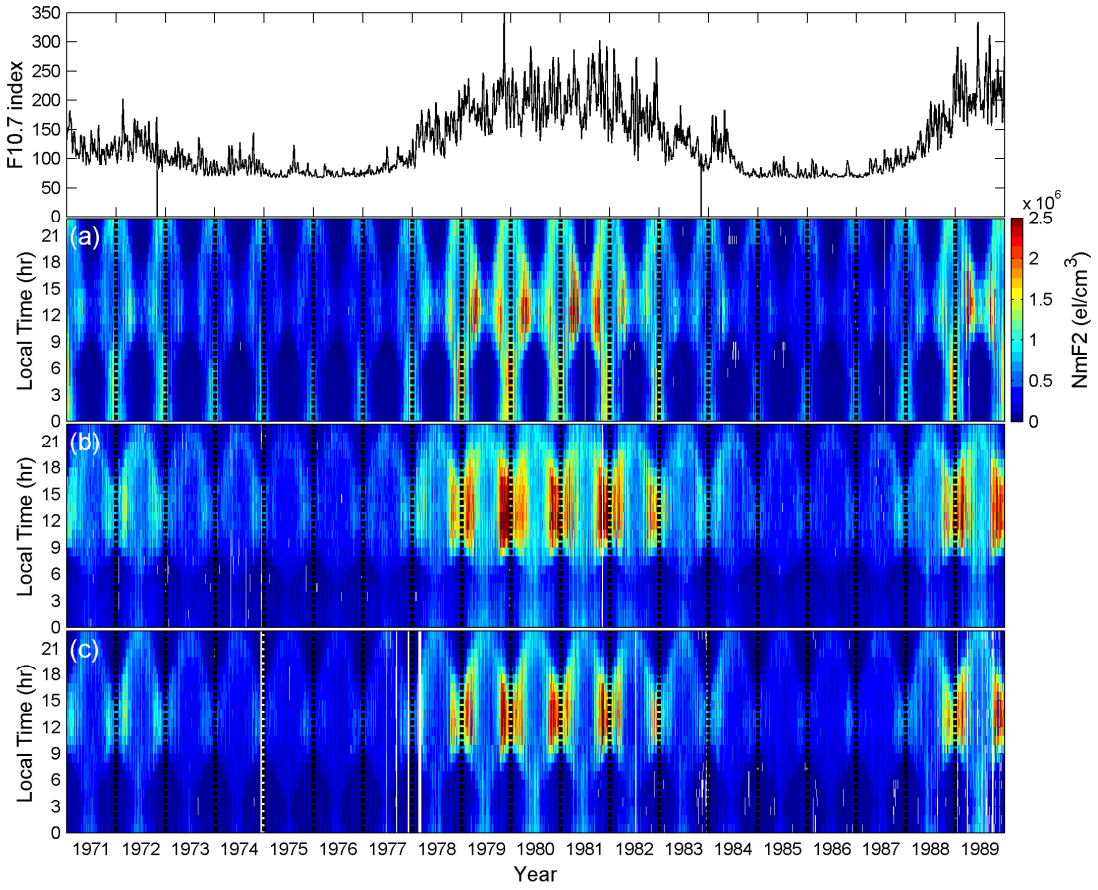


**Figure 2.** The daily variations of the 10.7 cm solar radio flux, F10.7 index (in unit of $10^{-22}$Wm$^{-2}$Hz$^{-1}$), and the NmF2 at (a)AIJ6N, (b)LN047, and (c)MG560 stations during 1971 to 1989.

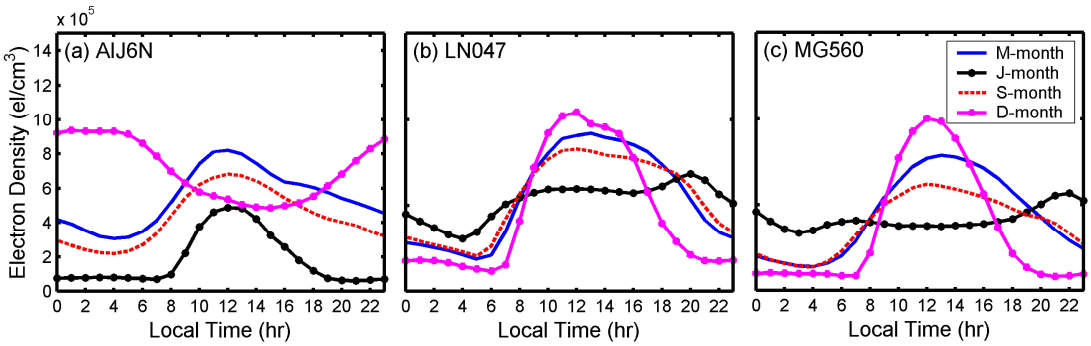


**Figure 3.** Monthly variation of diurnal NmF2 at (a) AIJ6N, (b) LN047, and (c) MG560 stations in M-month (blue line), J-month (black-dot line), S-month (red dash line), and D-month (pink-dot line).

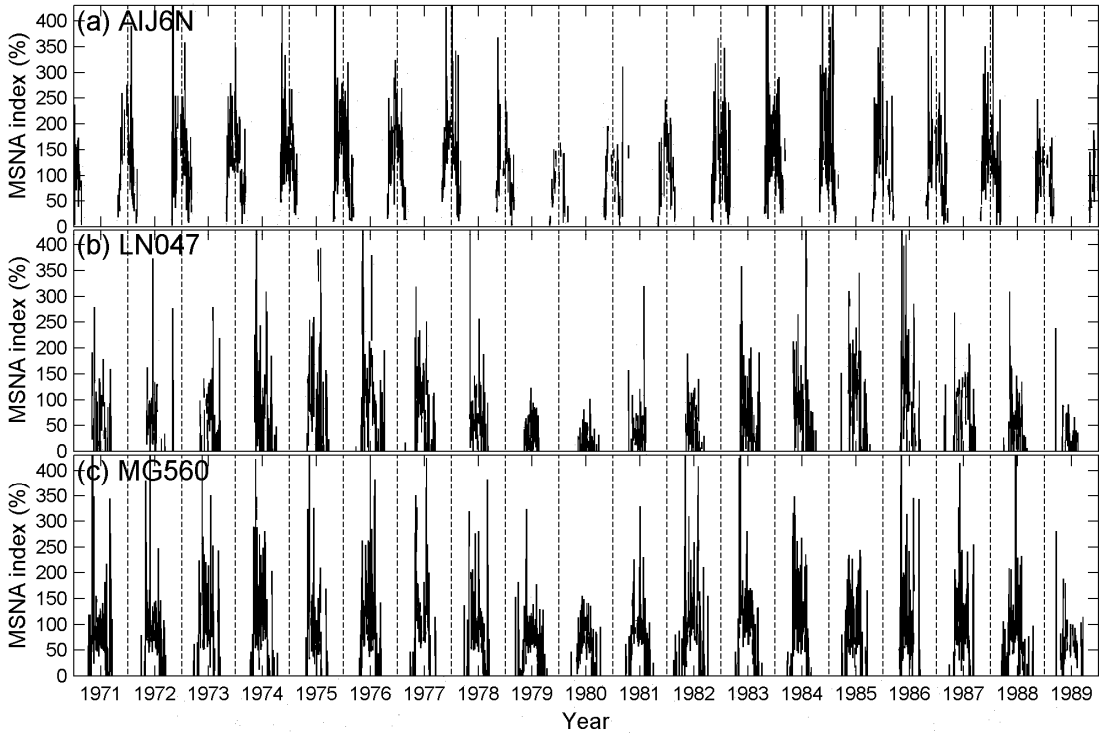


**Figure 4.** Daily variations of the positive MSNA index at (a) AIJ6N, (b) LN047, and (c) MG560 stations during 1971 to 1989.

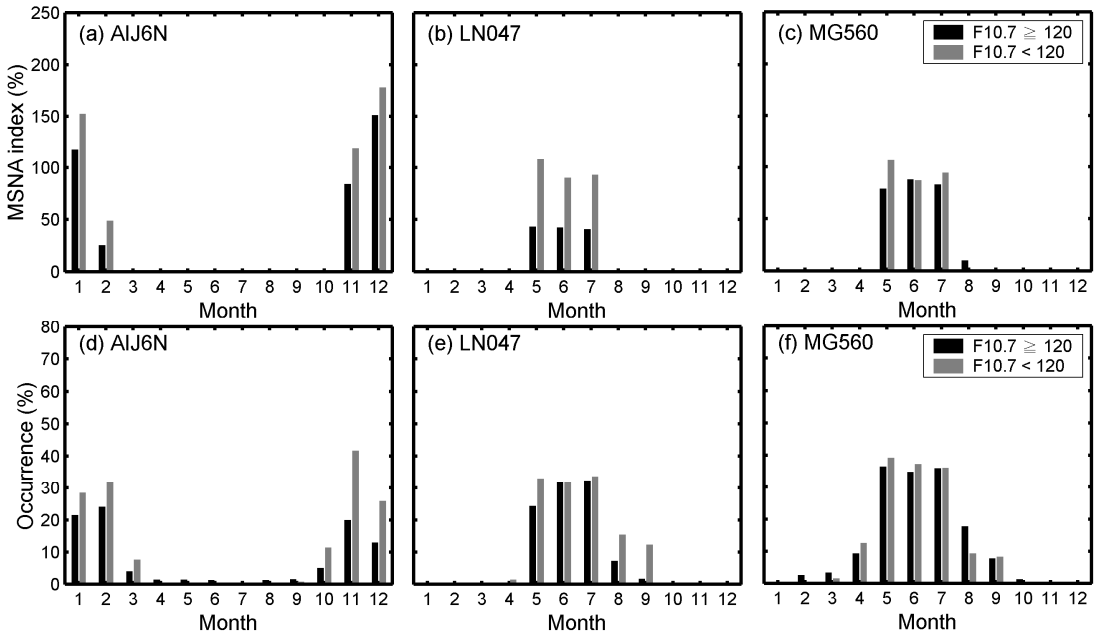


**Figure 5.** Monthly variation of MSNA index values and MSNA occurrence rates. The monthly variation of MSNA indexes are shown at (a) AIJ6N, (b) LN047, and (c) MG560 stations in different solar activity conditions. Black bars indicate the high solar activity (F10.7 ≧ 120) data and gray bars indicate the low solar activity (F10.7 < 120) data. The monthly occurrence rates of MSNA are shown at (d) AIJ6N, (e) LN047, and (f) MG560 stations in different solar activity conditions. Black bars indicate the high solar activity (F10.7 ≧ 120) data and gray bars indicate the low solar activity (F10.7 < 120) data.

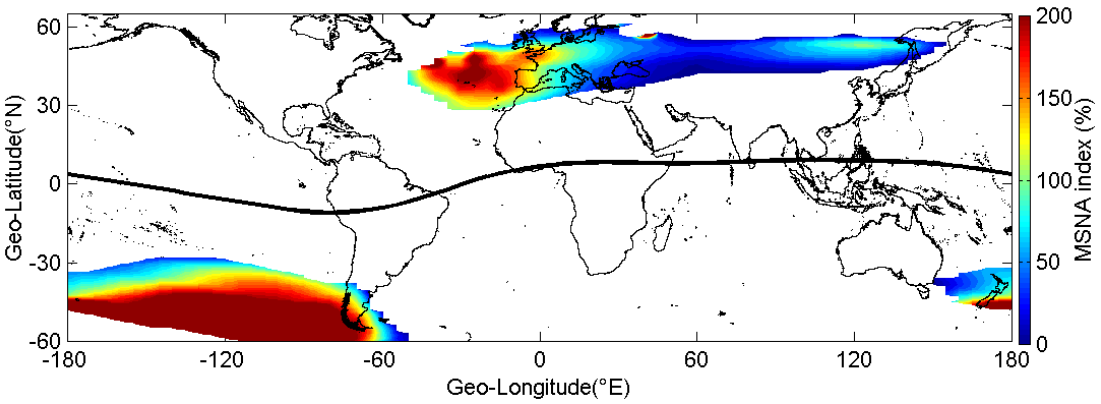


**Figure 6.** Global MSNA index during local summer days (Jun.16 for the northern hemisphere and Dec. 16 for the southern hemisphere) simulated by SAMI2 model. The black line indicates the geomagnetic equator.

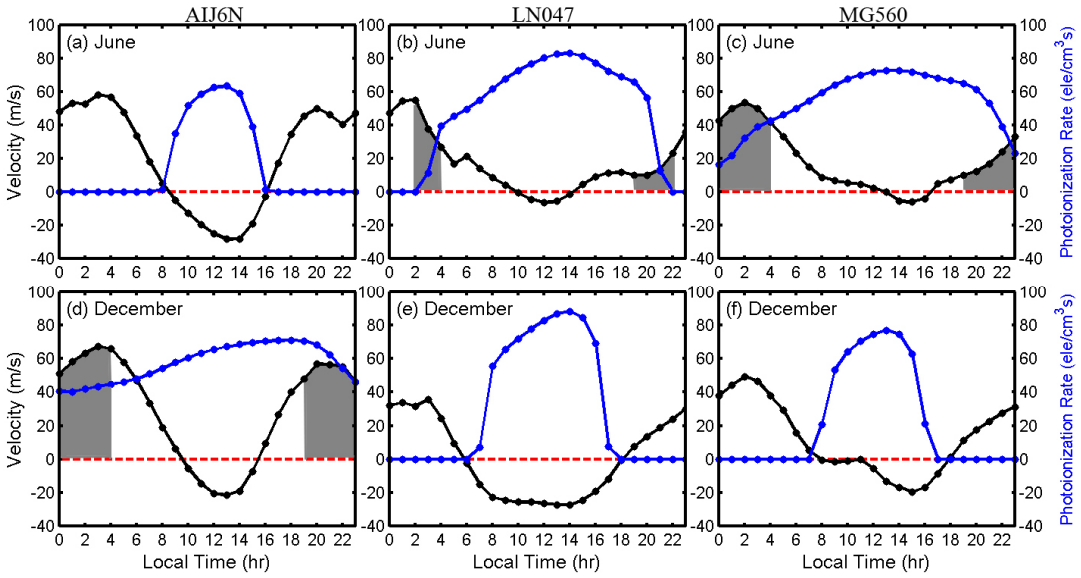


**Figure 7.** Hourly variation of vertical neutral wind and photoionization rate. Top panels show the results at (a) AIJ6N, (b) LN047, and (c) MG560 stations in June month. Bottom panels show the results at (d) AIJ6N, (e) LN047, and (f) MG560 stations in December month. Black-dot lines and associated left-side y-axis indicate the vertical neutral wind. Blue-dot lines and associated right-side y-axis indicate the photoionization rate. Gray region indicate the ionization-uplift effect with upward neutral wind and positive photoionization rate.

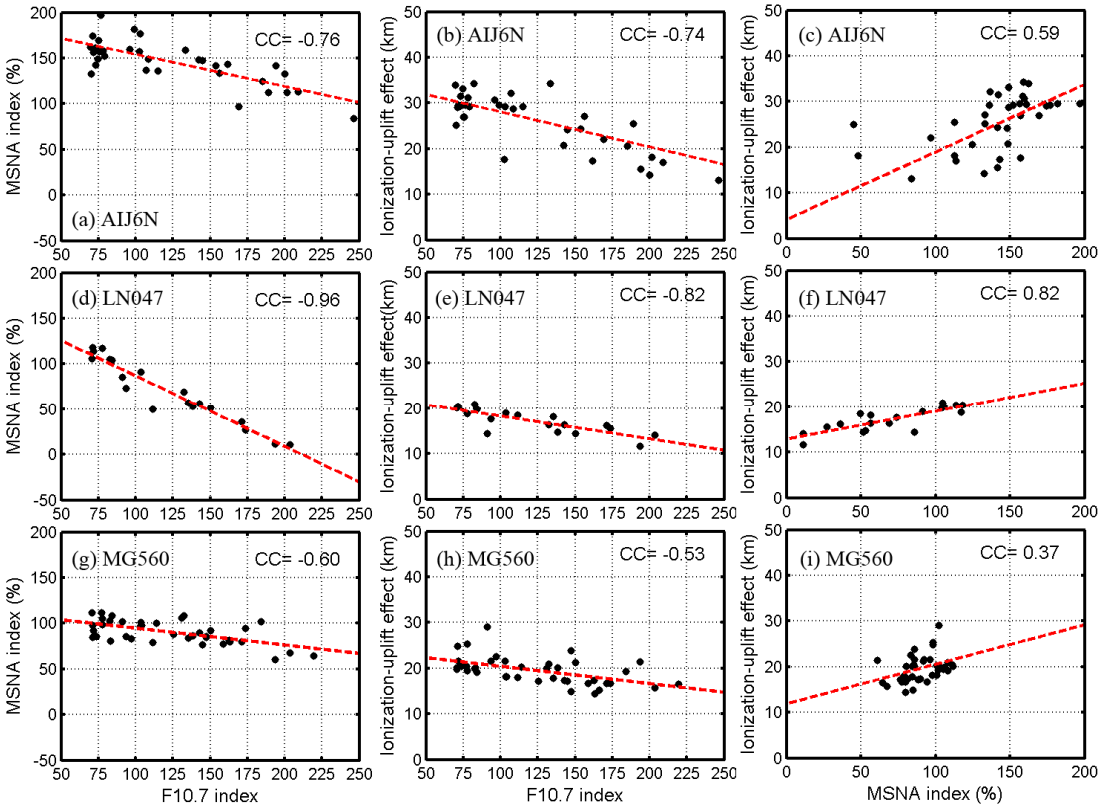


**Figure 8.** Solar activity variations of the MSNA index and the ionization-uplift effect. The top three panels indicate the results at AIJ6N station (a-c). The middle three panels indicate the results at LN047 station (d-f). The bottom three panels indicate the results at MG560 station (g-i). The solar activity dependences of the MSNA index and the ionization-uplift effect are shown in the left three panels and the middle three panels, respectively. The relationship between the MSNA index and the ionization-uplift effect are shown in the right three panels. Red dash-lines indicate the linear regression lines and CC indicates the correlation coefficient.

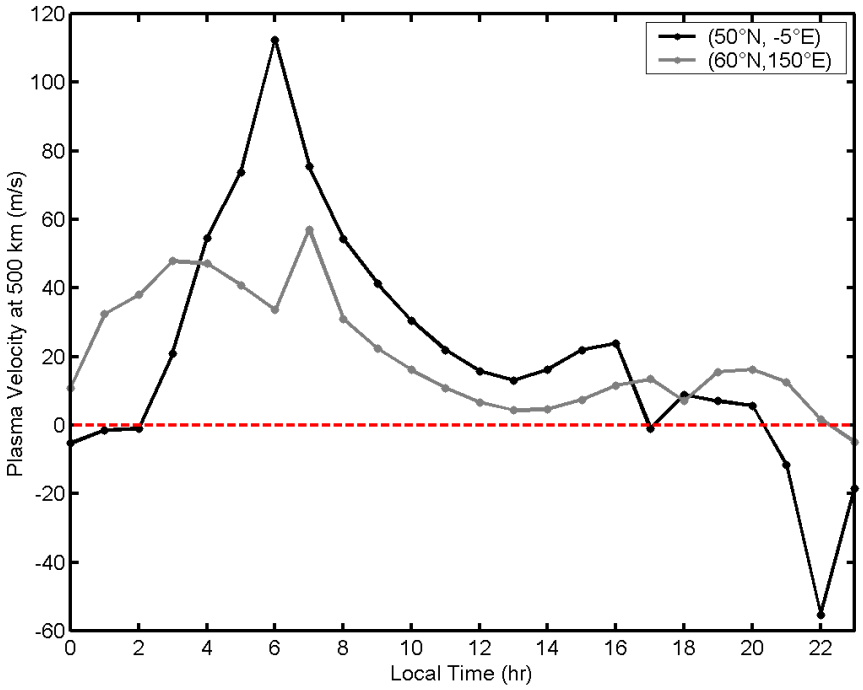


**Figure 9.** Plasma velocities at 500 km altitude at European and Northeast Asian locations on Jun. 16 in 2007 by SAMI2 model. The black-dot and gray-dot lines indicate the data at (50°N, -5°E) and (60°N, 150°E), respectively. Positive/negative value means the up/downward velocity.

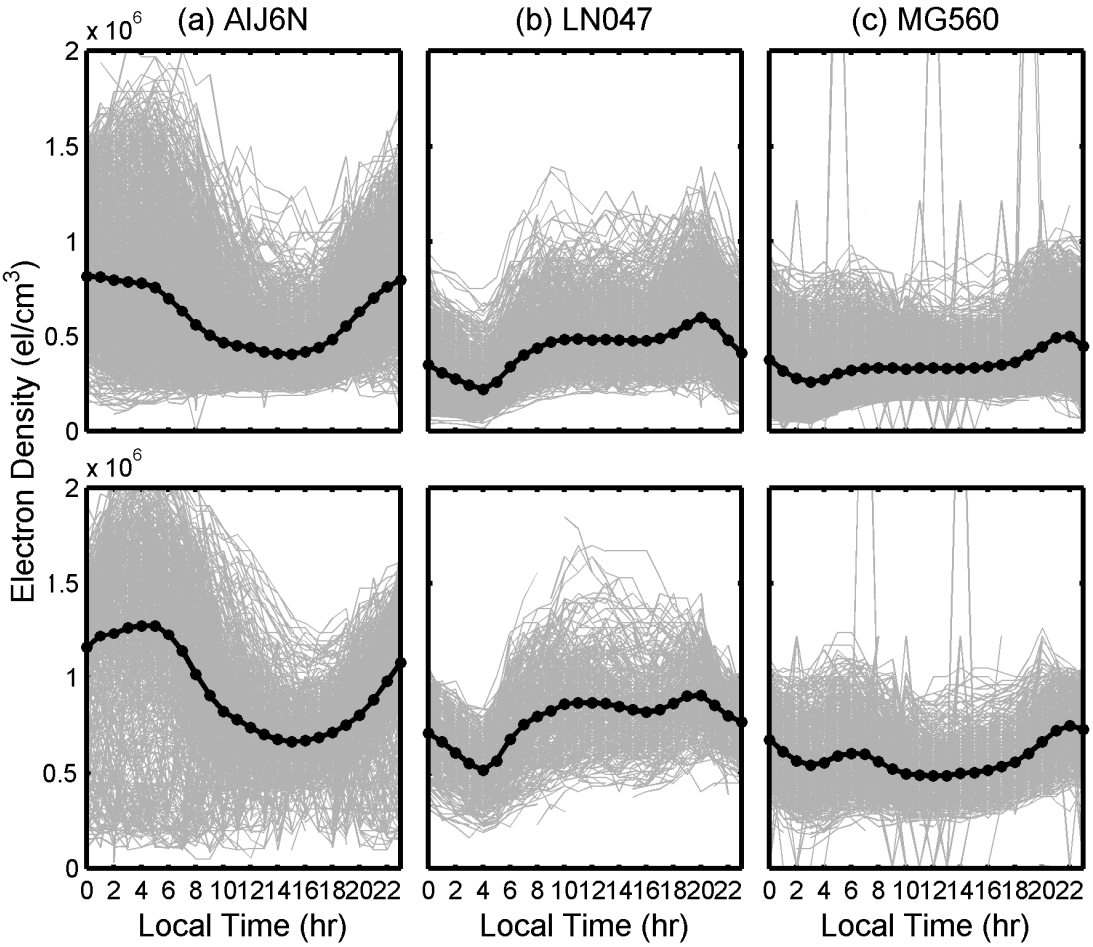


**Figure A1.** The daily variation of *NmF2* (in gray lines) during the local summer months and its average value (black-dot lines) at low solar activity (F10.7 index smaller than 120, top three panels) and high solar activity (F10.7 index larger than 120, bottom three panels) at AIJ6N, LN047, and MG560 stations.